Modeling Directional Two Arm Archimedes Spiral Coils in the RF Electromagnet Range

Anthony J. Kalinowski and Jason Maguire
Naval Undersea Warfare Center/Div. Npt. , Newport, RI 02841-1708

Abstract: The paper addresses a class of problems for modeling and consequently simulating the electromagnetic field radiation pattern from a two arm Archimedes spiral coil. The application considered is to have this flat double spiral coil embedded at the interface between two dielectric materials (i.e. the spiral is in a plane parallel to the interface layer), wherein each layer (referred to as *outer* and *inner*) has its own relative permittivity ε^o_r and ε^i_r. The performance of particular interest is knowledge of the radiated magnetic field **H** and electric field **E** in the neighborhood of the coil. The base legs of the two arms of the coil are driven independently by voltages V1 and V2, via impedance *lumped ports* of the type available in COMSOL. The radiation pattern can be steered in a plane parallel to the upper and lower layer interface by changing the ratio of V1/V2 and/or phase of V1 compared to V2. Further it is shown that the radiation can be confined in the inner layer by appropriately adjusting the permittivity ratio $\varepsilon^i_r / \varepsilon^o_r$ between the outer and inner layers.

Keywords: Electromagnetic Radiation, FEM modeling of coils.

1. Introduction

The application of interest herein, is to radiate strong magnetic fields in a two-layered dielectric medium. Of particular interest, is the situation where most of the electromagnetic radiated field is kept within the inner layer. Voltage driven flat coils have been selected as the radiator, because they nicely lie along the interface between the two dielectrics (typically solid materials). The paper treats the problem of solving for the driven radiated electric **E** field and magnetic **H** field emanating from a two arm Archimedes spiral coil as illustrated by the model shown in Fig. 1. This type coil has been used as an antenna as discussed for example, in Ref.[1]. The polar form of the radius R of the first arm of the coil centerline is variable and unfolds according to the relation

$$R(\theta)=R_o+R_o\,\theta \qquad \text{Eq (1)}$$

where θ is the cylindrical coordinate angle, and R_o is an off set constant starting radius at $\theta = 0$. A second arm can be created by rotating a copy of the first arm by 180^o .

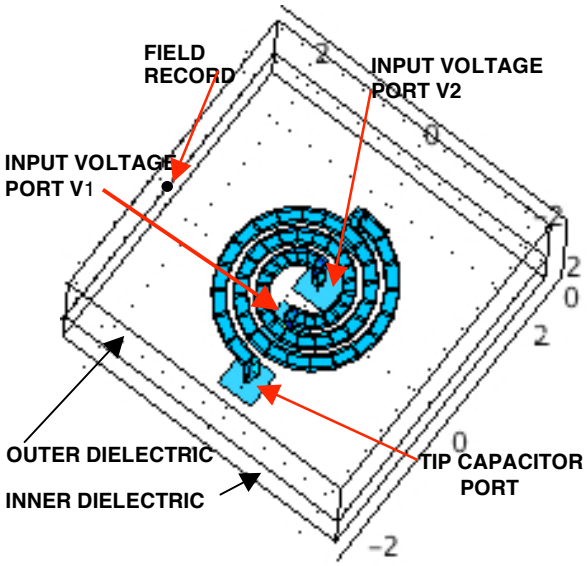

Figure 1. Isolated 2 arm Archimedes spiral Coil Model

The paper will pass through a sequence of increasingly complex problems, that illustrate what elements affect the strength and shape of the radiated magnetic **H** field pattern of the surrounding near field:

(a) basic circular spiral (e.g. Fig. 1)
(b) effect of feed line input port impedance Z_p
(c) effect of inner dielectric permittivity ratio, $\varepsilon^i_r / \varepsilon^o_r$, for the problem type shown in Fig. 1
(d) effect of coil geometry (circular spiral vs. elliptical spiral)
(e) variation of arm 1 feed voltage (V1) magnitude and phase vs. arm 2 feed voltage (V2) magnitude and phase, while holding total feed voltage |V1|+|V2|=constant.

1.1 Past Works

The response to spiral coils of the type considered herein (e.g. Fig. 1), is a complicated 3D field that is well beyond closed form

analytical solutions. There are two competing numerical methodologies for solving Maxwell's equation in the RF domain, where the physical size of the electromagnetic components (e.g. coils, and capacitors) are on the order of the electromagnetic medium wave length λ:

$$\lambda = c_o/(f\sqrt{\mu_r\varepsilon_r}) \quad \text{Eq(2)}$$

where co is the speed of light in vacuum, f is the wave frequency, ε_r is the relative permittivity, and μ_r is the relative permeability. The two candidate techniques are the finite element method (FEM) Ref.[2] and the finite difference method (FDM) Ref.[3]. The FEM has the advantage that it is more readily applied to situations where the configuration has irregular shaped obstacles, and therefore COMSOL was selected as the computational program for solving the problem at hand.

2. Governing Equations

The governing equations for the total electric field **E** in the dielectric domain (for time harmonic type response) are given by Maxwell's equations:

$$\nabla\times(\mu_r^{-1}\nabla\times\mathbf{E}) - k_0^{\,2}(\varepsilon_r - \frac{i\sigma}{\omega\varepsilon_0})\mathbf{E} = \mathbf{0} \quad \text{Eq(3)}$$

and are solved for **E** using the RF module in COMSOL.

2.1 Surface Boundary Conditions

The mesh termination at outer boundaries of the FEM model shown in Fig. 1 must include some sort of radiation absorbing boundary condition. Two types were considered, namely the PML (perfectly matched layer), and COMSOL's built in scattering boundary condition (used herein), namely: $nx(\nabla xE) - iknx(Exn) = 0$. For interfaces between two unlike materials, such as between the outer and inner dielectric as shown in Fig. 1, the continuity boundary condition of $nx(E_{out} - E_{in}) = 0$ is used.

The copper wire that makes up the coil is not modeled directly in the usual finite element sense (i.e. with a distribution of 3-D solid elements all the way through the thickness of the coil). The surface currents are limited to a very thin region ("skin effect as described in Ref.[2]), so instead, the copper coil is modeled with an equivalent surface impedance boundary condition applied only to the surface of the wire. The coil wire is therefore modeled as a "*wormhole*" passing through the dielectric medial, where the copper surface impedance boundary condition is applied at these wormhole surface elements, and is implemented as standard boundary condition offered within the COMSOL menu list of applicable boundary conditions.

Finally, the input voltage needs to be applied into the base of the coil (labeled as *input voltage port V1* and *input voltage port V2* in Fig. 1). New to the RF module, is the ability to avoid complex modeling of an actual input wire with some Z impedance rating, which is replaced with a COMSOL "*lumped port*" boundary condition. This amounts to modeling a planar rectangular tab that connects from the end of the coil –to-some sort of grounding plane (e.g. one the four square appearing feet at the base of the Fig. 1 model). Note there are two feet for the drive ports and two for the capacitor-loaded tips. The square feet of these grounding planes are also modeled with a copper surface impedance boundary condition like the wormhole surface.

2.2 Lumped Port Boundary Conditions

Here we address the parameter assignments applied to the lumped ports. This is where three items are assigned:

i) the voltage input feed (optional), $V = V_o e^{i\phi\pi/180}$, where V_o is the voltage input and ϕ is the phase angle in degrees.

ii) port type (uniform selected here)

iii) Lumped port impedance Z_{ref} (real for resistance and imaginary for capacitance)

2.3 Mesh sizing

For harmonic steady state problems, the mesh size is set according to the shortest wavelength expected during the event. For example, if N_{ew} is the number of elements/wave length required for accurate modeling and C_{min} is the slowest wave speed, and f_{max} the largest frequency experienced in a frequency sweep, then the mesh can be sized with $\Delta_{min} = C_{min} / (N_{ew} f_{max})$, (e.g. N_{ew} =6 for quadratic element shape functions).

3. Applications

Here we give examples of the five problem types (a,b,c,d,e) outlined in the introduction section.

3.1 basic circular spiral model

Here we define the basic model configuration before any variations in parameters are introduced. The overall model domain size is small (.05 cm x .05 cm x .04 cm), however the frequencies are high ($O(10^{11})$), where the RF wavelengths are on the order of the coil diameter of D=.03 cm . Our interest herein is mainly on the relative **H** field shapes (i.e. relative based on variation of the parameters specified in the problem types {a,b,c,d,e} and on the spatial range of the radiation **H** and **E** fields). The same shape sensitivities scale upward to larger dimensions, but with lower frequencies (assuming the electromagnetic material constants do not appreciably change with frequency). For example, in the models shown later, if S=100 is the dimension scale factor, multiplying all dimensions by S and multiplying the frequency by 1/S produced essentially the same shape radiation fields.

Geometry parameters flat circular spiral coil

The centerline of the coil is given by Eq(1) with the offset parameter R_o = .01 cm with a coil thickness of 0.02 cm. However with this thickness coil, the coil is too thick near the origin where external coil surfaces across from each other can overlap. Therefore the starting angle in the coil spiral is set at $\theta_s=\pi$, where θ is swept out for $\theta_s \le \theta \le \theta_s + 3\pi$. The R(θ) sweep for the circular spiral centerline is shown later in Fig. 8b. With this non zero θ_s , the starting spiral radius becomes $(1+\pi)\ R_o$, and surface overlap problems are eliminated .

Location of flat spiral coil

The location of the flat coil is positioned between the two dielectrics, with the coil thickness located within the inner dielectric. Later results showing side views (e.g. Fig. 6a) illustrate the depth location more clearly.

Material parameters:

The following material parameters were used for as the *base case starting parameters* of interest to this work:

Relative to the Fig. 1 model:

Outer Diel. $\varepsilon^o_r = \varepsilon_B$;

Inner Diel. $\varepsilon^i_r = .75\varepsilon_B$;

thus $\varepsilon^i_r / \varepsilon^o_r = .75$

Cu Coil $\varepsilon^c_r = 1.0$; $\mu^c_r = 1.0$; $\sigma^c_r = 6.0e7$[S/m]

Coil Voltage Arm Loading

The *base case* coil lumped port loading was for unit voltage and zero phase:

$V_1=1.0\ \phi_1=0$ deg. and $V_2=1.0\ \phi_2=0$ deg.

Lumped Port Impedances

Arm Drive ports 1 and 2 Zp=50 Ω

Arm Tip Ports 3 and 4 $Zp=-i\omega/C$

where C=tip capacitor input.

Solver Method

Three-dimensional problems rapidly become unmanageable unless measures are taken to deal with large degree of freedom models. Most of the models are run with 1/2 -to- 2/3 million unknowns on a 4G memory UNIX based operating system. Direct solvers run out of memory for our size problems, and therefore advantage of memory friendly iterative solver (GMRES) are employed, using a *geometric multigrid preconditioner* (right handed), a *SOR vector presmoother*, a *SORU vector postsmoother* and a *SPOOLS coarse solver*. These worked fine as long as the mesh had a reasonable number of elements/wavelength distribution. For example 1/2 million unknowns often reach convergence in approximately 4 min. per frequency.

Field Response Recording

The tangential component of the magnetic field ,H_t, in the X-Y plane of the spiral flat coil is the electromagnetic field quantity selected for display. The **H** field tends to propagate out radial from the center of the coil, where the strongest component of the **H** vector is tangent to the cylindrical coordinate r direction centered at the coil center, namely H_t. The field variables computed are the Cartesian components of **H,** so the XY plane H_t component is post-processed according to

$$H_t = \frac{yH_x}{\sqrt{x^2+y^2}} - \frac{xH_y}{\sqrt{x^2+y^2}} \qquad \textbf{Eq(4)}$$

where the H_x and H_y coefficients are simply sin and cos rotation quantities. We note that when a record point like the one labeled "FIELD RECORD" in Fig. 1 lies along the x axis (x=0), then by Eq(4), H_t and H_x are equal. In all the field plots shown later: (a) the frequency sweep plots are taken at the Fig. 1 "FIELD RECORD"

point (which is slightly below the bottom plane of the spiral coil as shown by a "bullet marker" in a model side view in Fig. 6a, and (b) all x-y plane planar contour plots are in the inner dielectric, at a sliced plane located at the bottom thickness of the spiral coil. The dominant motion is outward propagating curved wave fronts from the coil center, where like EM wave planar fronts, the E_z component of the electric field **E** (which is ⊥ to H_t) is similar in shape to H_t (but not shown herein).

3.2 Effect of Feed Line Port Impedance Z_p

Early on it was discovered that in order to achieve stronger radiated fields in the plane near the interface between the two dielectrics, two quantities had to be changed beyond the base case described in section 3.1, namely the drive port impedance Zp from 50 to .05 and the inner dielectric to outer dielectric ratio ε^i_r / ε^o_r from the base case value of .75 to 1.5 . The 1.5 ratio was achieved by simply doubling the inner dielectric base case $\varepsilon^i_r = 2x\varepsilon_B$. Later in section 3.3 we show why the doubling was preferred.

The response point for the field measurements was taken at the point marked "FIELD RECORD" in Fig. 1. The results shown in Fig. 2 are using the double base case $\varepsilon^i_r / \varepsilon^o_r = 1.5$ and is swept vs. frequency for three values of Zp = {.05 1, 50}.

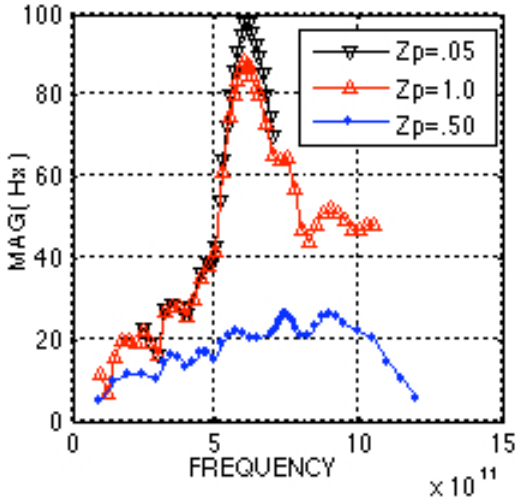

Figure 2. Mag(Hx) vs. Frequency Taken at Boundary Point "FIELD RECORD" for Three Zp Values, with $\varepsilon^i_r / \varepsilon^o_r = 1.5$

The goal is to maximize the strength of the radiated H field, therefore the Zp=.05 value leads to the port impedance with the sharpest resonance peak. The resistance in the field behaves like damping, and thus smaller Zp values lead to stronger resonances.

3.3 Effect of Doubling Inner Dielectric Permittivity Magnitude

The goal here is to keep most of the radiated magnetic field within the inner dielectric. The initial trials that used the base case material constants, lead to a greater percentage of the **H** field being propagated upward through the outer dielectric. It was found that by increasing the inner dielectric permittivity by a factor of two substantially improved the situation.

In terms of a coil diameter-to-wavelength ratio R=D/λ , for the double base case of $\varepsilon^i_r / \varepsilon^o_r = 1.5$, $R^i \approx 1.5$ for the inner dielectric and $R^o \approx 1.2$ for the outer dielectric. Therefore the peak responses occur when the magnetic wavelengths are on the order of the coil diameter.

3.3.1 Frequency sweep: $\varepsilon^i_r/\varepsilon^o_r$ comparisons

For example the Fig. 3 frequency sweep plot for the Mag(Hx) showed that at f=6.0e11 Hz, a substantially lower magnitude is experienced for the base case, compared to the double base case. This is due in part to the resonance shifting, but even at the shifted resonance peak frequency of f=6.5e11, the base case peak is still much smaller than the double base case.

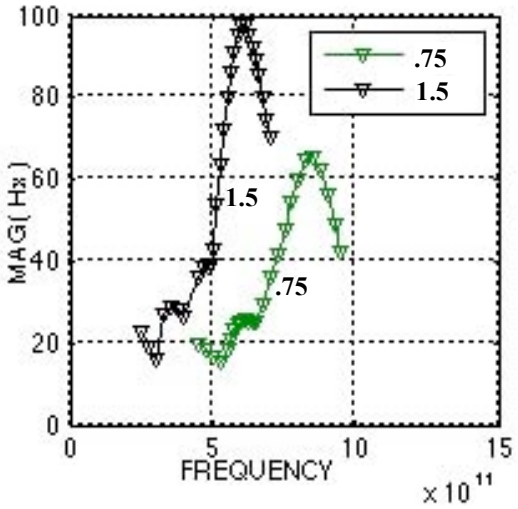

Figure 3. **Mag(Hx) vs. Frequency Taken at Boundary Point "FIELD RECORD" for Zp=.05 and for Base Case ∇ $\varepsilon^i_r / \varepsilon^o_r = .75$ and Double Base Case ∇ $\varepsilon^i_r / \varepsilon^o_r = 1.5$**

3.3.2 Full field H_t radiation pattern

Next a full field surrounding the rectangular base case Fig. 1 model is added so that a better view of the radiated field is observed.

In the full field model of Fig. 4 (and subsequent ones) for example, one can still see the see the original rectangular domain outline of Fig. 1, before the outer far field circular domain was added. This interface is not a physical one but is simply a mathematical interface connecting two zones made of the same material, where the continuity boundary condition is applied at the internal interface.

The real part of the complex magnetic H_t field is plotted instead of the magnitude, so that the sign change of the $\mathbf{H_t}$ roll off with increasing radial component from the coil center, illustrates a traveling wave like structure of the magnetic field. The white zones of this plot (and all others to follow in the paper), indicate that the plotted quantity is beyond the outer extremes of the color legend (e.g. as one might expect the strongest part of the field is closest to the coil and therefore appears white).

The Fig. 6 result, shows a side-by-side YZ vertical plane comparison of the base case $\varepsilon^i_r / \varepsilon^o_r = .75$ and the double base case $\varepsilon^i_r / \varepsilon^o_r = 1.5$.

The figure illustrates that as the radiated field progresses away from the coil, it tends to stay mainly confined to the inner dielectric as shown in the Fig. 6b plot.

The "bullet marker" in the Fig. 6a plot shows the depth marker where the Figs. 2,3 and 9 frequency sweep data was taken on the rectangular Fig. 1 model.

3.3.3 Surface current density on coil

Finally the surface current density $Js = Js_x i + Js_y j + Js_z k$ on the surface of the coil is of particular interest. The plot in Fig. 7 illustrates the magnitude of this vector (A/M) in a bird's eye view looking down the z-axis.

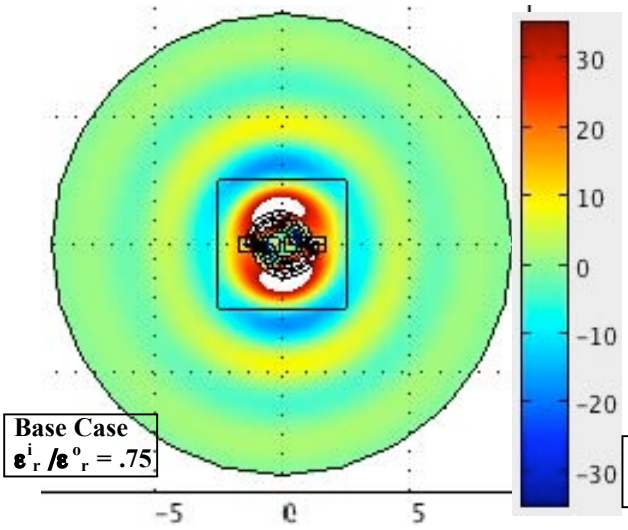

Figure 4. RePt (H_t) in Horizontal XY Plane, Base Case $\varepsilon^i_r / \varepsilon^o_r = .75$ at f=6 e11Hz.

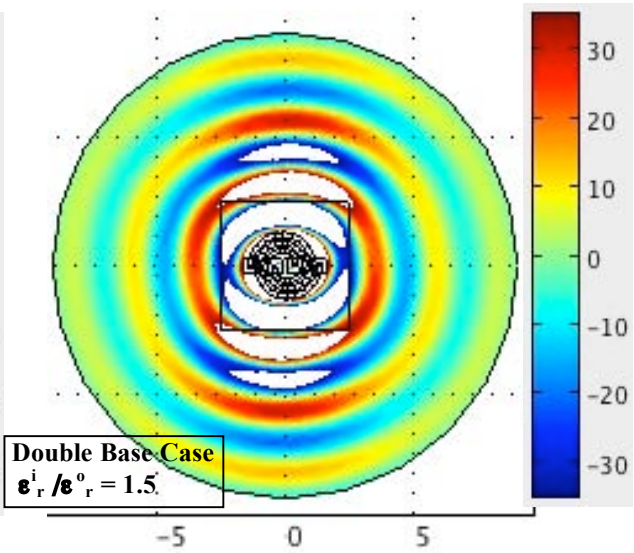

Figure 5. RePt(H_t) in Horizontal XY Plane, Double Base Case $\varepsilon^i_r / \varepsilon^o_r = 1.5$ at f=6 e11Hz.

Upon comparing the XY planar results of Fig. 4 compared to Fig. 5, we clearly see that the double base case $\varepsilon^i_r / \varepsilon^o_r = 1.5$, results in a stronger radiated magnetic field which is consistent with the Fig. 3 curve results as well.

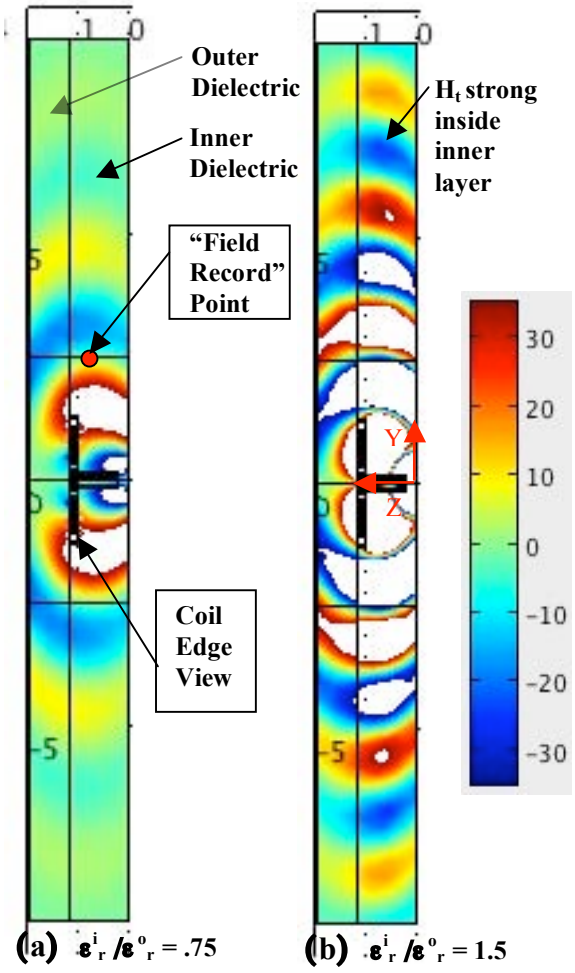

Figure 6. RePt(Ht) in Vertical YZ Plane; Base Case $\varepsilon^i_r/\varepsilon^o_r$ =.75 vs. Double Base Case $\varepsilon^i_r/\varepsilon^o_r$ = 1.5, at f=6 e11Hz

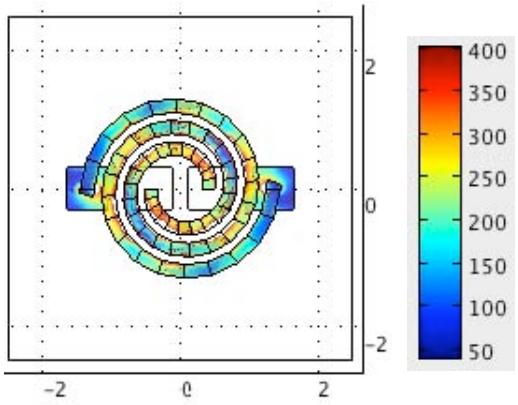

Figure 7. Surface Current Density Mag(Js) A/M on the surface of the Coil, Double Base Case $\varepsilon^i_r/\varepsilon^o_r$ = 1.5, at f=6 e11Hz.

3.4 Effect of Coil Geometry (Circular Spiral vs. Elliptical Spiral)

Next we consider the effect of the coil cross sectional shape on the radiated magnetic field. The motivation here is the potential of having some unusual radiation effects, such as having a stronger focused beam in the Y direction. The equation for the spiral centerline, given by Eq(1) , is modified by replacing the R_o with R'_o

$$R(\theta) = R'_o + R'_o\,\theta \qquad \text{Eq (5)}$$

where:

$$R'_o = \sqrt{\frac{(\alpha R_o)^2}{1-\cos(\theta)^2(1-\alpha^2)}}$$

with α=(semi-minor axis) / (semi-major axis) of base ellipse, and R_o is the same value used in the circular Eq(1). The R'_o formula, is the polar form of an ellipse for radius vs. θ. As in the circle spiral, we use the same offset parameter R_o=.01 cm with a coil thickness of 0.02 cm, α=.75 and a starting angle in the coil spiral of $\theta_s=\pi$, where θ is swept out for $\theta_s \le \theta \le \theta_s + 3\pi$. We note that Eq(5) reduces to Eq(1) when $\alpha \to 1.0$. The resulting spiral ellipse centerline vs. spiral circular centerline comparison is shown in Fig. 8b and the corresponding finite element geometrical block segments filled out about the centerline (before filling with finite elements) is shown in Fig. 8a.

3.4.1 Ellipse spiral frequency sweep: The resulting frequency sweep solution for the selected variable Mag(Hx) taken at boundary point "FIELD RECORD" for lumped input port impedance Zp=.05 and double base case $\varepsilon^i_r/\varepsilon^o_r$ = 1.5 is shown in Fig. 9. The corresponding circular spiral case is shown for comparison on the same plot, where it is seen that the peak resonance for the ellipse spiral is slightly higher and occurs shifted to the right at at f=6.5e11Hz , compared to at f=6.0e11Hz for the circular spiral.

3.4.2 Ellipse spiral radiation patterns at resonance: The ellipse spiral radiation pattern for the H_t tangential component of the **H** magnetic field at the ellipse spiral peak resonance of f=6.5e11Hz is of interest here. The data is presented in two formats, where the first

Fig. 10 result is for the real-part(H_t) in the horizontal XY plane, double base case $\varepsilon^i_r / \varepsilon^o_r$ = 1.5**;** and the second Fig. 11a result is for the for Mag(H_t)**.** The effect of the ellipse spiral vs. circular spiral for the real-part(H_t) can be observed upon comparing each at their peak resonance (i.e. Fig. 5 vs. Fig. 10). The ellipse spiral peak-to-peak wave maximums in the radial direction appear closer spatially (since the frequency is higher), and also the beam width in the Y direction appears to be a little narrower. This beam narrowness of the main lobe in the Y direction can be better observed by comparing the ellipse spiral Mag(H_t) in Fig. 11a to the

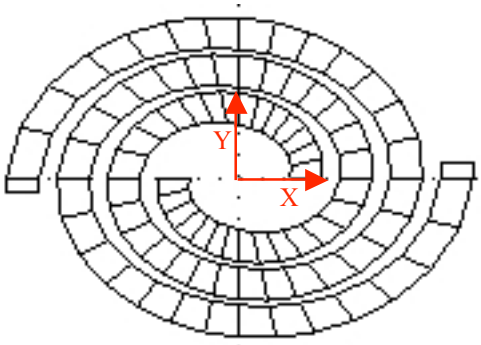

a) XY View of Ellipse Spiral Coil Shape α=.75

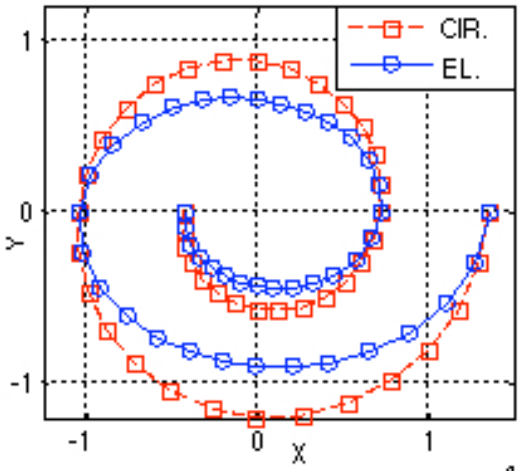

b) Circle (α=1.0) vs. Ellipse (α=.75) Spiral Centerline

Figure 8. Ellipse Coil Cross Section

corresponding Mag(H_t) circular spiral counterpart (shown later in Fig. 12). The ellipse spiral has a stronger main lobe as can be seen by comparing the position of the Mag(H_t) =35 (white border fringe) location indicated at the tip of the ∇ markers on both figures (Fig. 11a vs. Fig. 12). We also point out that the ellipse coil is achieving a greater Mag(H_t) strength with less

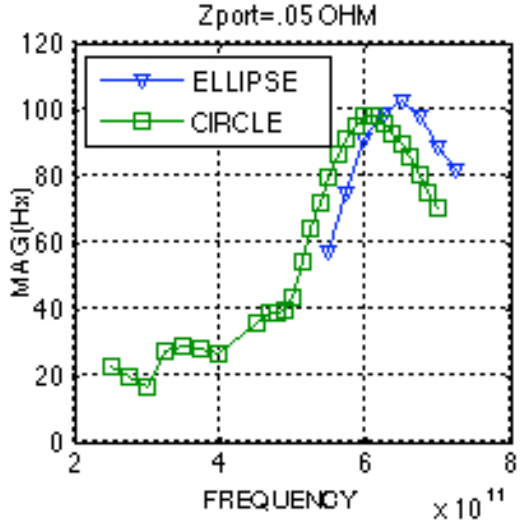

Figure 9. Circle vs. Ellipse for Mag(Hx) vs. Frequency Taken at Boundary Point "FIELD RECORD" for Zp=.05 and Double Base Case $\varepsilon^i_r / \varepsilon^o_r$ = 1.5

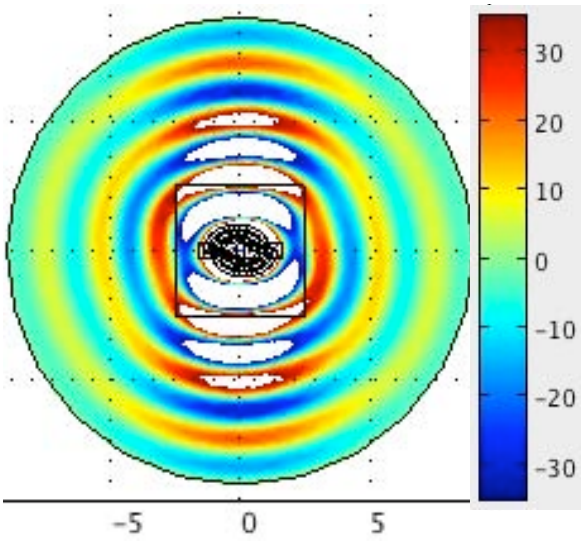

Figure 10. Ellipse Coil: RePt(H_t) in Horizontal XY Plane, Double Base Case $\varepsilon^i_r / \varepsilon^o_r$ = 1.5 at f=6.5 e11Hz.

material as can be seen by comparing the ellipse spiral centerline arc length vs. the circular spiral arc length as in Fig. 8b. The ratio of arc lengths

is (ellipse spiral arc length)/(circle spiral arc length) ≈ 0.86 .

3.4.3 Ellipse spiral radiation patterns at off ellipse resonance f=6.0e11Hz: The radiation pattern for the for the Mag(H_t) tangential component of the **H** magnetic field at the off ellipse peak resonance of f=6.0e11Hz in horizontal XY plane, double base case $\varepsilon^i_r / \varepsilon^o_r$ = 1.5 is of interest here. Based on the Fig. 9 frequency sweep curves, at f=6.0e11Hz , we also expect the ellipse spiral to have a smaller strength field strength than at the peak f=6.5e11Hz, which is confirmed by observing the full field plots Fig. 11b vs. Fig. 11a .

.

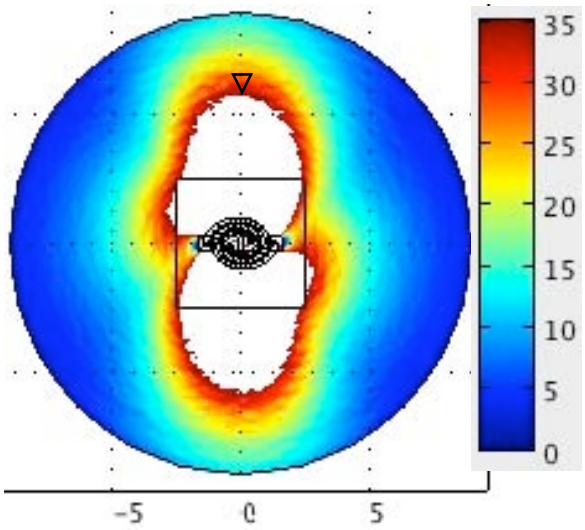

a) f=6.5 e11Hz

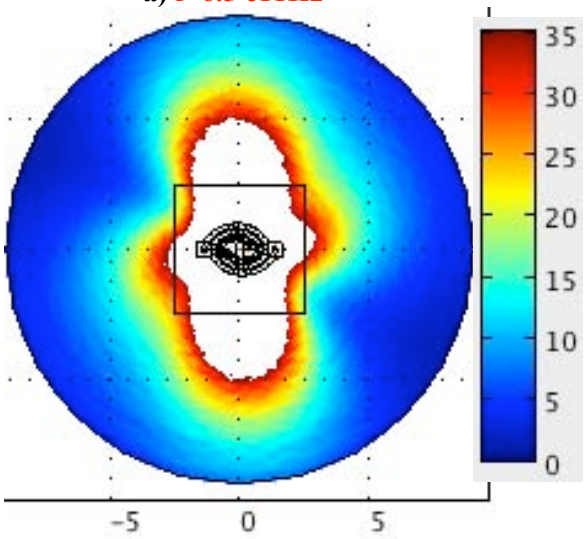

b) f=6.0 e11Hz

Figure 11 Ellipse Coil: Mag(H_t) in Horizontal XY Plane, Double Base Case $\varepsilon^i_r / \varepsilon^o_r$ = 1.5

3.4.4 Ellipse vs. circular spiral radiation patterns at same frequency f=6.0e11Hz: The radiation pattern for the Mag(H_t) for the ellipse spiral vs. circular spiral *at the same frequency* in horizontal XY plane, for double base case $\varepsilon^i_r / \varepsilon^o_r$ = 1.5 is of interest here. The frequency of f=6.0e11Hz is significant, because recall that this is the frequency where the circular spiral peaks out. Therefore the comparison shows what effect the ellipse vs. spiral shape has on the beam patterns and can be observed by comparing Fig. 11b vs. Fig. 12. The Fig. 9 frequency sweep plot shows that at f=6.0e11Hz, the ellipse response is off its peak, therefore the fact that the ellipse spiral shows a weaker Fig. 11b **H** field than the circular spiral Fig. 12 **H** field is consistent data.

3.5 Variations of Arm 1 Feed Voltage V1 (Phase and Magnitude) vs. Arm 2 Feed Voltage V2 (Phase and Magnitude)

The idea here is to investigate the feasibility of redirecting the beam pattern electronically without having to physically rotate the coil. Thus we are concerned with altering the H field beam patterns by making variations on the coil's feed line input. In particular, the variation of arm 1 (feed voltage V1 and phase ϕ_1) vs. arm 2 (feed voltage V2 and phase ϕ_2), while holding total feed voltage available |V1|+|V2|=constant.
This constant was taken at 2 volts, where the base case we have used up until now is recall: V_1=1.0 ϕ_1=0° and V_2=1.0 ϕ_2=0° . In all the variation examples to follow we use only the circular spiral coils, with the same dimensions etc. used in the previous sections. The double base case $\varepsilon^i_r / \varepsilon^o_r$ = 1.5 permittivity is also used throughout this section 3.5 and all runs are made at the same frequency of f=6.0e11 Hz.
The results in this section display plots of the smoother Mag(H_t) quantity, but sacrifice the wave roll off features brought out when real-part(H_t) is plotted. Beam patterns are more easily seen with the Mag(H_t) plot format.

3.5.1 V_1=1.0 ϕ_1=0°; V_2=1.0 ϕ_2=0°

This first case *with balanced feed line parameters* V_1=1.0 ϕ_1=0°; V_2=1.0 ϕ_2=0° serves as a base line example for later examples. The results shown here in Fig. 12 are an exact repeat of the Fig. 5 case already discussed in section 3.3 except here, we plot the smoother Mag(H_t) quantity rather than the real-part(H_t). Note that in the Fig. 12 result shows most of the field strength is up- down (± Y direction).

3.5.2 V_1=1.0 ϕ_1=0°; V_2=1.0 ϕ_2= -180°

This next case is with *balanced voltage and unbalanced phase* feed line parameters V_1=1.0 ϕ_1=0°; V_2=1.0 ϕ_2= -180° serves as an example where we change only the phase of the input lines, leaving the magnitudes still balanced. The results show the interesting effect that most of the radiated field is sent to the left-right (± X direction), with very little sent in the vertical up-down (± Y direction).

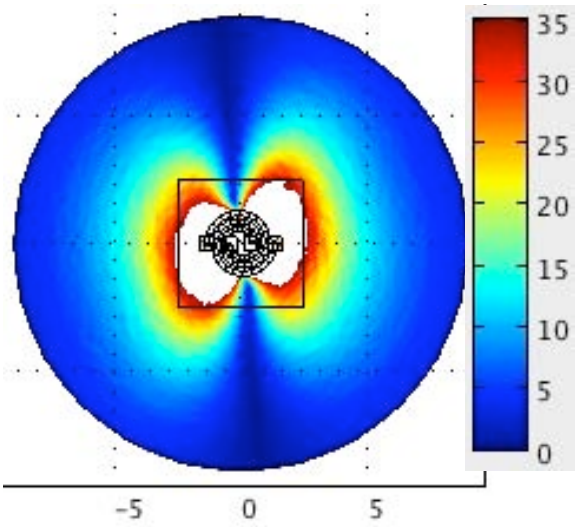

Figure 13. Mag(H_t) in Horizontal XY Plane, Double Base Case $\varepsilon^i_r / \varepsilon^o_r$ = 1.5; V_1=1.0 ϕ_1=0° and V_2=1.0 ϕ_2=-180° at f=6 e11Hz

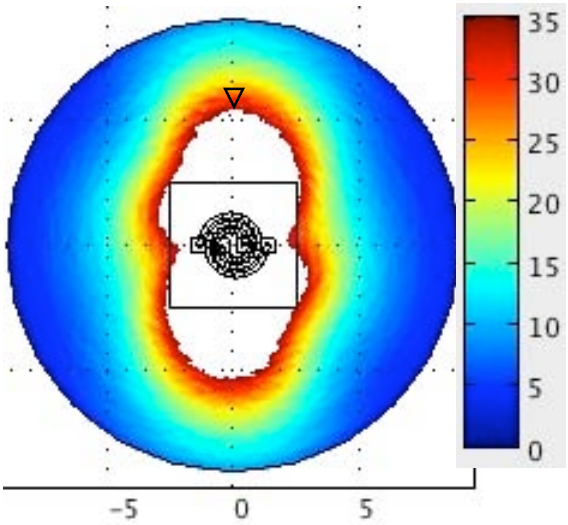

Figure 12. Mag(H_t) in Horizontal XY Plane, Double Base Case $\varepsilon^i_r / \varepsilon^o_r$ = 1.5 ; V_1=1.0 ϕ_1=0° and V_2=1.0 ϕ_2=0° at f=6 e11Hz

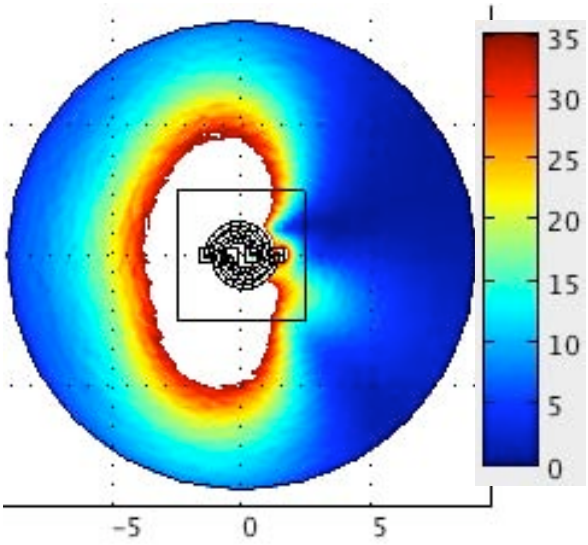

Figure 14. Mag(H_t) in Horizontal XY Plane, Double Base Case $\varepsilon^i_r / \varepsilon^o_r$ = 1.5; V_1=0.5 ϕ_1=0° and V_2=1.5 ϕ_2=-90° at f=6 e11Hz

3.5.3 $V_1=0.5\ \phi_1=0°; V_2=1.5\ \phi_2= -90°$

This final case is with both *unbalanced voltage and unbalanced phase* feed line parameters $V_1=0.5\ \phi_1=0°$; $V_2=1.5\ \phi_2= -90°$ serves as an example where we change both the phase of the input lines, and change the magnitudes as well, while keeping the net feed voltage still at 0.5+1.5=2.0 volts total. The results show the interesting result that most of the radiated field pattern is directed to the third and fourth quadrants. This could be of used when one does not want radiation in the first and second quadrant say, to protect radiation sensitive neighboring components.

4. Conclusions

The results in this paper illustrate how COMSOL is used to solve for the radiated electromagnetic fields in the 3-D space surrounding the flat spiral coils, in a RF frequency range where the dimensions of the coil are on the order of an electromagnetic wavelength. The results show that by altering the shape of the spiral coils (circular vs. elliptical) and by varying the amplitude and phase of the two arm coil feed lines, it is possible to distort the shape and direction of the radiated field, such as pointing the radiation away from a particular direction, such as in Fig. 14 where most of the radiation is confined to the third and fourth quadrant of the XY plan view of the radiation field. Also we showed by appropriately adjusting the permittivity ε^{i}_{r} / ε^{o}_{r} ratio of the inner-to-outer dielectric layers, most of the radiation was confined to the inner layer away from the coil.

References

1. Johnson, Richard C., Antenna Engineering Handbook, Third Edition, McGraw Hill, Inc., NY, 1993.

2. Jim Jianming, The Finite Element Method in Electromagnetics, Second Edition, John Wiley and Sons, 2002

3. NguTaflove Allen and Susan C. Hagness Susan (2005). *Computational Electrodynamics: The Finite-Difference Time-Domain Method, 3rd ed.*. Artech House Publishers.

4. COMSOL Inc. (www.comsol.com)

9. Acknowledgements

This work was sponsored by the Naval Undersea Warfare Center's In-house Laboratory Independent Research Program. The author would also acknowledge the RF model set up help received from COMSOL staff member Bjorn Sjodin and 3-D coil geometry modeling from Vineet Dravid.